UNIVERSITY of York

This is a repository copy of *Guided mode resonance sensor for the parallel detection of multiple protein biomarkers in human urine with high sensitivity*.

White Rose Research Online URL for this paper:
https://eprints.whiterose.ac.uk/157280/

Version: Accepted Version

Article:
Kenaan, Ahmad, Li, Kezheng, Barth, Isabel et al. (3 more authors) (2020) Guided mode resonance sensor for the parallel detection of multiple protein biomarkers in human urine with high sensitivity. Biosensors and Bioelectronics. 112047. ISSN 0956-5663

https://doi.org/10.1016/j.bios.2020.112047

Reuse
This article is distributed under the terms of the Creative Commons Attribution-NonCommercial-NoDerivs (CC BY-NC-ND) licence. This licence only allows you to download this work and share it with others as long as you credit the authors, but you can't change the article in any way or use it commercially. More information and the full terms of the licence here: https://creativecommons.org/licenses/

Takedown
If you consider content in White Rose Research Online to be in breach of UK law, please notify us by emailing eprints@whiterose.ac.uk including the URL of the record and the reason for the withdrawal request.

White Rose university consortium
Universities of Leeds, Sheffield & York

eprints@whiterose.ac.uk
https://eprints.whiterose.ac.uk/

Guided mode resonance sensor for the parallel detection of multiple protein biomarkers in human urine with high sensitivity

*Ahmad Kenaan[1,2], Kezheng Li[2], Isabel Barth[2], Steven Johnson[3], Jie Song[1]& Thomas F. Krauss[2]**

[1]Institute of Nano Biomedicine and Engineering, Shanghai Engineering Research Centre for Intelligent Diagnosis and Treatment Instrument, Department of Instrument Science and Engineering, School of Electronic Information and Electrical Engineering.
Shanghai Jiao Tong University, Shanghai 200240, P.R. China
Email: sjie@sjtu.edu.cn

[2] Department of Physics, University of York, York YO10 5DD, UK.
Email: thomas.krauss@york.ac.uk

[3]Department of Electronic Engineering, University of York, York YO10 5DD, UK
Email: steven.johnson@york.ac.uk

Keywords: immunosensor, optical biosensor, protein biomarkers, guided mode resonance, polyethylene glycol, urine matrix.

Abstract

The rising cost of global healthcare provision and new approaches to managing disease are driving the development of low-cost biosensing modalities, such as label-free photonic methods based on dielectric resonances. Here, we use the combined sensing and imaging capability of a guided mode resonance (GMR) sensor to detect multiple biomarkers (troponin, procalcitonin and C-Reactive Protein) in parallel in undiluted urine samples. A key requirement of such a biosensor is the simple and direct functionalization with suitable antibodies to ensure the disease-specific detection of protein biomarkers. Here, antibodies were immobilized using a succinimidyl-[(N-maleimidopropionamido)-hexaethyleneglycol] ester ($SM(PEG)_6$) spacer. The polyethylene glycol (PEG) chemistry enables low detection limits of 10 pg mL^{-1} or better for all protein biomarkers, while minimizing non-specific binding compared to more commonly used strategies such as (3-Aminopropyl)triethoxysilane (APTES) or dextran. Our approach supports the vision of a simple yet highly sensitive diagnostic platform that could be used for pre-screening patients for a wide range of diseases at point-of-care, thereby relieving the pressure on overstretched healthcare services.

1. Introduction

Early recognition and targeted treatment of disease is an essential element of healthcare provision. Being able to detect multiple biomarkers in a single test is particularly desirable, as it allows for a more accurate and personalised diagnosis or for screening for a wide range of diseases in a single test. Conducting such a test in a clinical matrix is essential and doing so in urine is particularly desirable as the sample can be collected non-invasively, which is preferred by patients. The challenge of using urine as a sample matrix is that the concentration of biomarkers is typically low; the physiological concentration of many proteins is 3-4 orders of magnitude lower in urine than in blood plasma (Eamudomkarn et al., 2018), which presents a major challenge to the sensing modality. For example, the cardiac biomarker troponin needs to be detected at levels of 10-40 pg mL^{-1} in urine for the sensor to be clinically relevant (Tanislav et al., 2016; Upasham et al., 2018).

Various sensor technologies have been developed to meet these demands, including electrochemical, calorimetric, piezoelectric, and optical biosensors (Kazemi-Darsanaki et al., 2013; Kenaan et al., 2016; Thakur and Ragavan, 2013; Thévenot et al., 2001). Biosensors based on optical transduction are particularly attractive as they offer high sensitivity, contact-free and simultaneous detection of multiple biomarkers. Furthermore, the refractive index sensitivity of photonic resonances can be exploited to enable label-free biomarker detection, further simplifying the diagnostic procedure. The diagnostic potential of resonant photonic sensors, such as those based on surface plasmon resonance (SPR), microring resonance or guided mode resonance (GMR) has already been demonstrated. While waveguide-based sensors such as microrings (Luchansky et al., 2010) and bimodal waveguides (Herranz et al., 2017) are the most sensitive amongst these, they require accurate alignment strategies in order to couple the light into the waveguide which makes them difficult to implement in low-cost, point-of-care solutions. In contrast, the leaky nature of

GMR-based biosensors means light can be coupled easily into the grating using a simple collimated beam. The key question is then whether the intrinsically low quality factor of the leaky mode approach prevents a sensor from achieving the high sensitivity required to detect disease biomarkers in urine?

The GMR sensing modality was first proposed by Wang and Magnusson (Wang and Magnusson, 1993), and demonstrated experimentally as fiber endface biosensor by Wawro (Wawro et al., 2000). Later, Cunningham et al. showed that the grating structure can be fabricated inexpensively by replica moulding or nanoimprint techniques (Cunningham, 2010). Recently, we introduced the chirped GMR approach (Triggs et al., 2017). The chirp translates spectral information into spatial position, so the refractive index change caused by molecular binding can be detected simply by imaging the spatial position of the optical resonance. This means that the bulky and expensive spectrometer typically required for monitoring the shift in optical resonance can be replaced with a simple, low cost camera. Here, we take this imaging capability one step further and demonstrate that multiple sensing areas can be monitored in parallel, thereby adding multiplexing capability (Fig. 1).

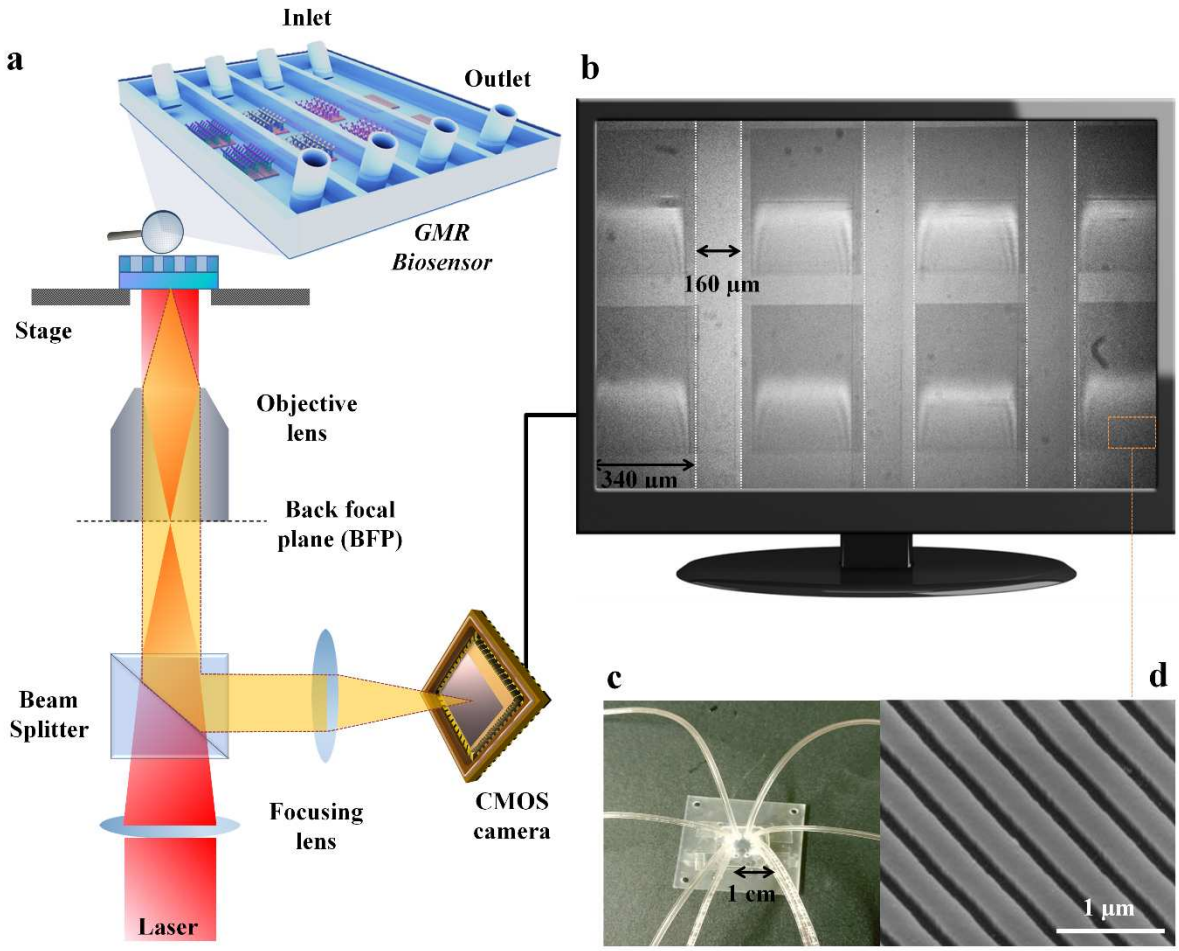

Fig. 1. Multiplexing capability of a chirped GMR sensor. a) Schematic diagram of the measurement setup showing the multiplexed chirped GMR consisting of four independent measurement channels. Three channels are functionalized with biomarker-specific antibodies, here C-reactive protein (CRP), troponin (TNNT1) and procalcitonin (PCT). The fourth channel is unfunctionalized and used as a reference to account for systemic drifts e.g. due to temperature. b) Field of view of the camera showing all 4 channels. Each channel contains two GMRs to provide redundancy and increase fidelity. c) The microfluidic channels are made of PDMS and are connected separately. d) SEM micrograph of the grating made in silicon nitride.

A GMR is a refractive index sensor that requires surface functionalization with a capture molecule, such as an antibody, to gain specificity. Limits of detection achieved so far using a functionalized chirped-GMR sensor are in the ng mL^{-1} range, which is comparable with other leaky-mode

105 modalities, e.g. plasmonic nanoholes (145 pg mL^{-1}) (Li et al., 2017). Nevertheless, in order to be
106 truly competitive with conventional diagnostics based on the enzyme-linked immunoassay
107 (ELISA), and to provide clinically relevant sensitivity, the sensor needs to demonstrate 1-10 pg
108 mL^{-1} sensitivity. Here, we demonstrate performance at this level by introducing an improved
109 functionalization protocol.

110 The key requirement for any functionalization protocol is high affinity binding to a particular target
111 molecule, coupled with the minimization of non-specific binding events which would otherwise
112 reduce the detection specificity. The latter requirement of non-specific binding is often overlooked;
113 many studies in the literature have been conducted with laboratory dilutions that avoid non-specific
114 binding simply by the absence of competing agents instead of by optimizing the protocol for real
115 sample matrices such as undiluted urine or blood. Furthermore, many protocols are carefully
116 optimized for a specific antigen/antibody pair. However, achieving high performance for
117 multiplexed detection without optimizing each assay is still a challenge.

118 The functionalization of dielectric or silicon surfaces used in photonic biosensors typically employ
119 silane chemistries to render the surface reactive against carboxylate or amine groups exposed on
120 an antibody surface (Vashist, 2012). For example, (3-Aminopropyl)triethoxysilane (APTES) is
121 commonly used to generate primary amine groups on the sensor surface to which the antibodies
122 are crosslinked via exposed carboxylate groups using the EDC/NHS chemistry (1-Ethyl-3-(3-
123 dimethylaminopropyl)carbodiimide/N-hydroxysuccinimide, resulting in the formation of a stable
124 amide bond. While simple and inexpensive, the amine coupling chemistry can lead to
125 multimerization of the activated antibodies that may mask its binding sites and introduce
126 conformational stress (Dixit et al., 2011; Stefansson et al., 2012), and lead to reduced specificity
127 due to non-specific binding to the free amine groups that have not been occupied by an antibody.

Moreover, the chain length of APTES is short resulting in steric hindrance that impedes antigen binding (Kim and Herr, 2013; Makaraviciute and Ramanaviciene, 2013). A longer, flexible spacer consisting of a hydrophilic, anti-fouling polymer is desirable in order to enable higher density immobilization of antibodies with steric freedom (Jönsson et al., 2008; Yakovleva et al., 2003). A common example of such a spacer is dextran, which provides a large volume of antibody binding sites because of its porous structure and its large molecular weight (Kim and Herr, 2013; Lee et al., 2013). Although the dextran matrix provides the sensor surface with a large number of binding sites, many of these sites can also cause significant non-specific binding, which is clearly undesirable.

Here, we exploit the commercially available $SM(PEG)_6$ spacer (succinimidyl-[(N-maleimidopropionamido)-hexaethyleneglycol] ester) as a crosslinker between the sensor surface and the antibody. PEG has previously been adopted to reduce steric hindrance, improve water solubility and reduce aggregation (Kim and Herr, 2013; Li et al., 2016; Nagasaki et al., 2007; Pochechueva et al., 2014; Weimer et al., 2000; Wen et al., 2009; Yuan et al., 2014). $SM(PEG)_6$ is a sulfhydryl and amine reactive heterofunctional polyethylene glycol (PEG) with N-hydroxysuccinimide (NHS) ester and maleimide groups at the termini. Maleimide terminated PEG is thiol-reactive which is used in our binding assay for bioconjugation with the sensor surface that has been thiolated using 3-Mercaptopropyl)trimethoxysilane (MPTS). This results in a surface functionalized with a monolayer of NHS esters which can form a covalent bond with free amines exposed on the antibody surface. We also note that the physical thickness of the SM(PEG)6 monolayer is < 3 nm, which is much shorter than the evanescent tail of the GMR mode of >100

nm (Drayton et al., 2019). We thus do not expect the SM(PEG)$_6$ spacer to adversely affect the sensitivity of the GMR. The functionalization protocol is illustrated in Fig. 2.

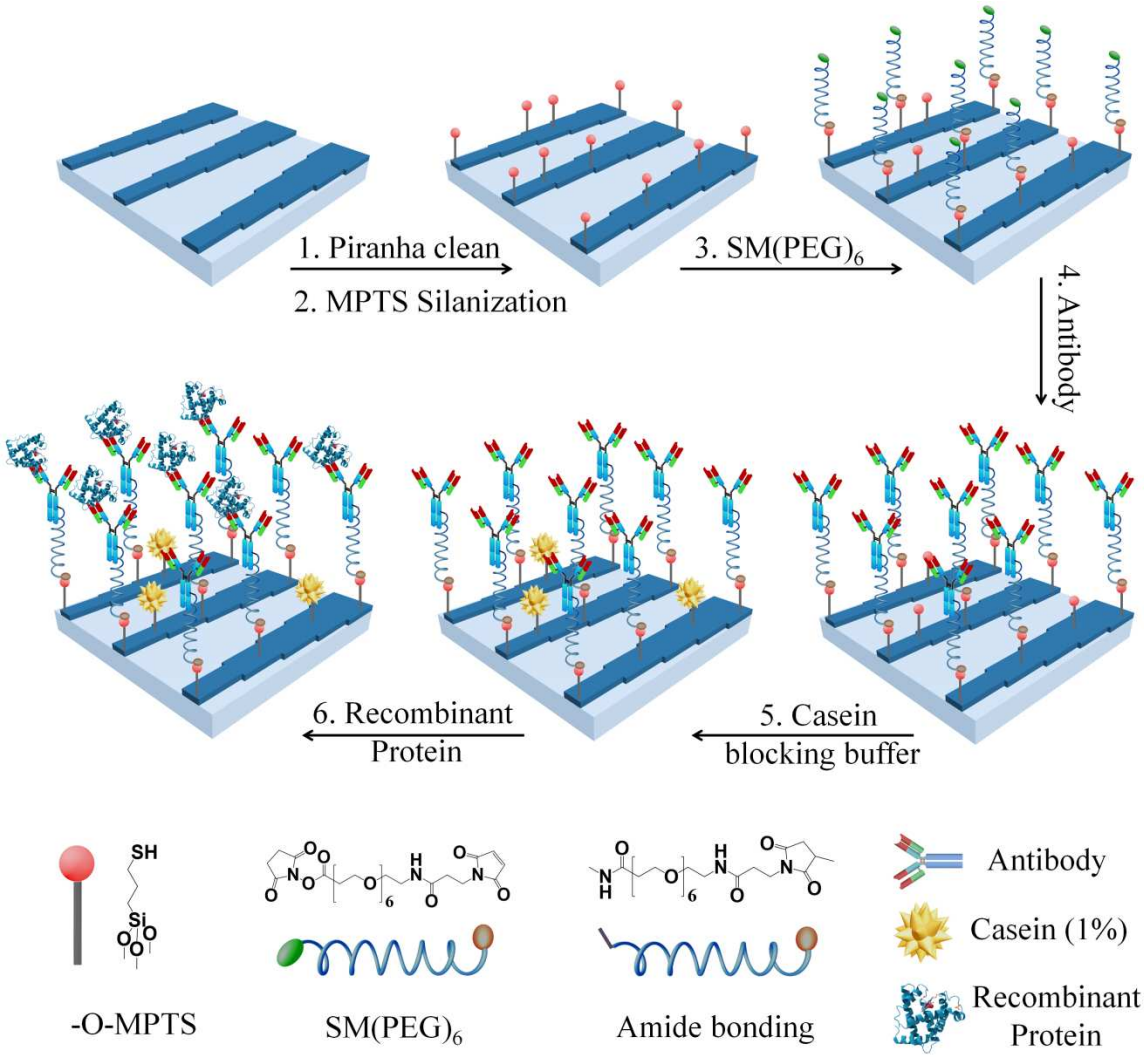

Fig. 2. Functionalization protocol using PEG as a spacer on a silicon nitride GMR. (1) Hydroxyl groups (OH) are introduced to the surface by piranha treatment. (2) Sulfhydryl groups are generated by (3-Mercaptopropyl)trimethoxysilane (MPTS) salinization for 7h. (3) SM(PEG)$_6$ crosslinkers are introduced to the sulfhydryl groups via the maleimide groups after incubation overnight in DMSO. (4) Antibody is introduced and immobilized on the PEGylated surface via its primary amine group to form an amide bond after 60 min of incubation. (5) Casein blocking buffer (1%) is added for ~30 min to block non-specific binding sites. (6) The Recombinant protein is added to the antibody sites at $T = 37^0$C. Steps 2-6 are performed inside the microfluidic channel.

2. Experimental section

Sub-sections regarding materials, chirped GMR fabrication, microfluidics, channels fabrication, and functionalization protocols including EDC/Sulfo-NHS, $SM(PEG)_6$, and Dextran chemistry are provided in the supplementary information file.

3. Results

3.1. Quartz crystal microbalance with dissipation (QCM-D) analysis

We first used a quartz crystal microbalance with dissipation (QCM-D) using silicon dioxide quartz sensor to optimize the functionalization protocol using an antibody against Immunoglobulin G (IgG) (anti-IgG) as an exemplar (see experimental methods for detail). QCM-D is a well-established reference tool that provides quantitative data, so is ideally suited for process development. A clear binding curve is observed as the anti-IgG immobilizes on the PEG spacer Fig. 3a. Upon saturation, the surface is washed with PBS to remove unbound antibodies, followed by flushing with casein buffer (1%) to block any remaining non-specific binding sites. We observe negligible binding of casein suggesting that the PEG forms a densely packed, anti-fouling monolayer. Finally, IgG is introduced into the QCMD flow cell leading to a clear binding curve. For comparison, the protocol was repeated for surfaces functionalized with APTES and dextran (see methods section and Fig. S2a and Fig. S2b for more detail). The specific and non-specific binding for these surfaces in comparison to the PEG functionalized sensor is quantified in Fig. 3b and Table S1. The shift in resonant frequency upon exposure to anti-IgG is highest for PEG, indicating a greater density of surface immobilized antibodies. This is mirrored by the IgG binding (red bars). Importantly, the amount of non-specific binding is smallest for the PEG functionalized surface (using casein as an indicator for non-specific binding). Overall, PEG offers the highest *specific* and the lowest *non-specific* binding of the three protocols, along with higher number of antibodies immobilized on the

surface (Fig. S2c and Fig. S2d), which is likely due to the minimization of steric hindrance coupled with the anti-fouling properties inherent to PEG monolayers. This combination of properties is critical for highly sensitive biomarker detection in a clinical matrix.

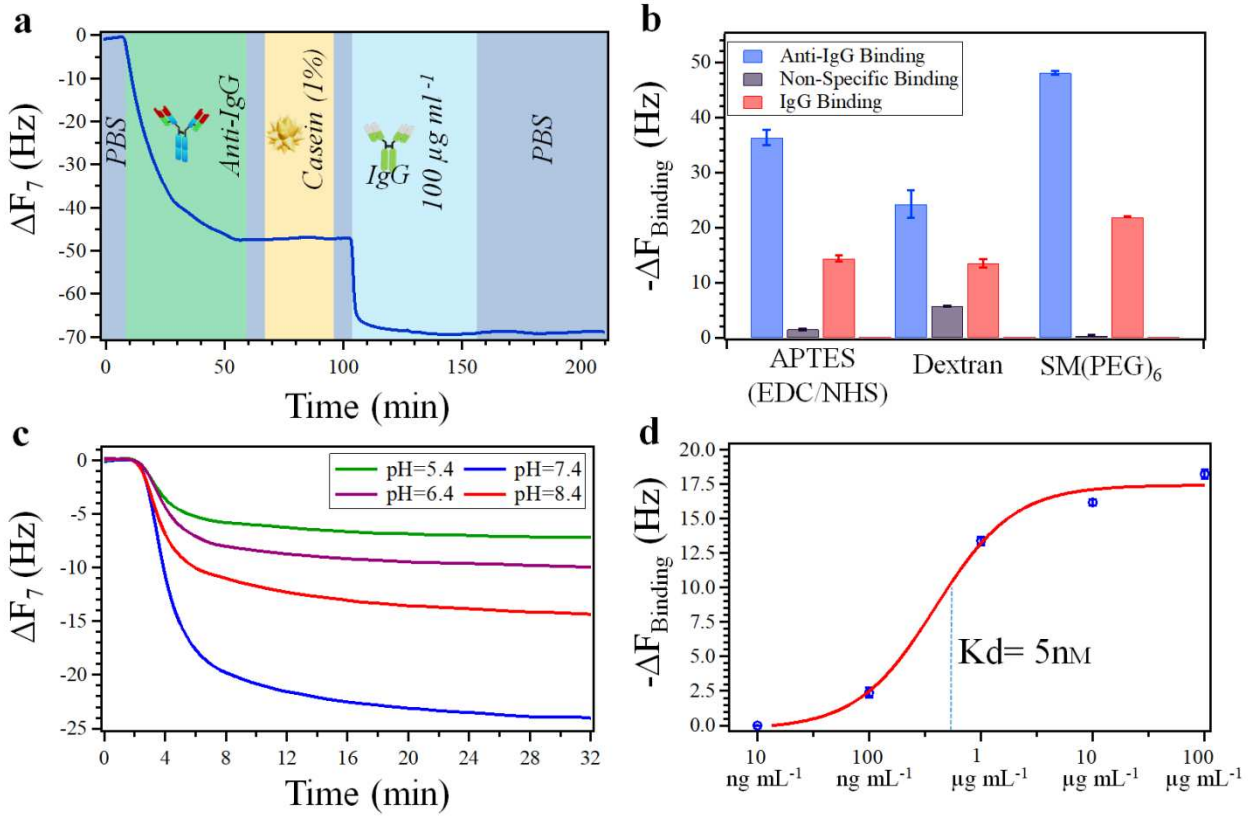

Fig. 3. Quartz crystal microbalance with dissipation (QCM-D) analysis. (a) IgG binding assay employing $SM(PEG)_6$ at pH = 7.4. (b) Comparison of the different functionalization protocols (APTES, Dextran and PEG) in terms of non-specific binding and in terms of frequency shift upon binding to IgG. Each point represents the mean ±SD of three replicates. (c) *pH* dependence on IgG binding. (d) IgG binding to the PEGylated surface as a function of concentration. Each point represents the mean ±SD of three replicates.

Fig. 3c shows the pH-dependence of binding between IgG and surface immobilized anti-IgG for a *pH* range between 5.4 and 8.4, which highlights the best performance at near neutral *pH* (maximum at *pH* = 7.4), in agreement with the results reported in the literature (Barnes, 1966; Hughes-Jones

et al., 1964; Yang et al., 2017). Finally, we examined the binding performance as a function of IgG concentration at *pH* = 7.4 for concentrations between 10 ng mL^{-1} to 100 µg mL^{-1} and observe a clear binding Langmuir isotherm (Fig. S2d), which allows us to determine a dissociation constant K_D of 5 nM (750 ng mL^{-1}), in close agreement with published values (~4 nM) (Kuo and Lauffenburger, 1993; Strauch et al., 2014).

3.2. Chirped guided mode resonance (GMR) analysis

Following the QCMD control experiments, we applied the PEG protocol to the chirped GMR sensor. The calibration indicates that a 1µm shift in position corresponds to $1.67x10^{-4}$ refractive index units (RIU) (Triggs et al., 2017). Given the noise figure of 0.35 µm (Fig. S3), this corresponds to a limit of detection of $5.8x10^{-5}$ RIU. Note that the results in Fig. 4 were all obtained in undiluted human urine adjusted to *pH* = 7.4. The full measurement sequence is shown in Fig. 4. After introducing the $SM(PEG)_6$ overnight to ensure the maximum coverage (Fig. S4), un-bound reagents are removed by a dimethyl sulfoxide (DMSO) wash, followed by drying with nitrogen gas. The surface is then exposed to PBS at *pH* = 7.4 to establish a baseline. Next, the antibodies are added (anti-IgG, anti-CRP, anti-PCT and anti-TNNT1) through the independent polydimethylsiloxane (PDMS) flow channels, followed by the casein blocker. A clear binding curve is observed associated with immobilization of the antibodies on the sensor surface. Again, we only observe a negligible shift in resonance following exposure to the casein blocker,

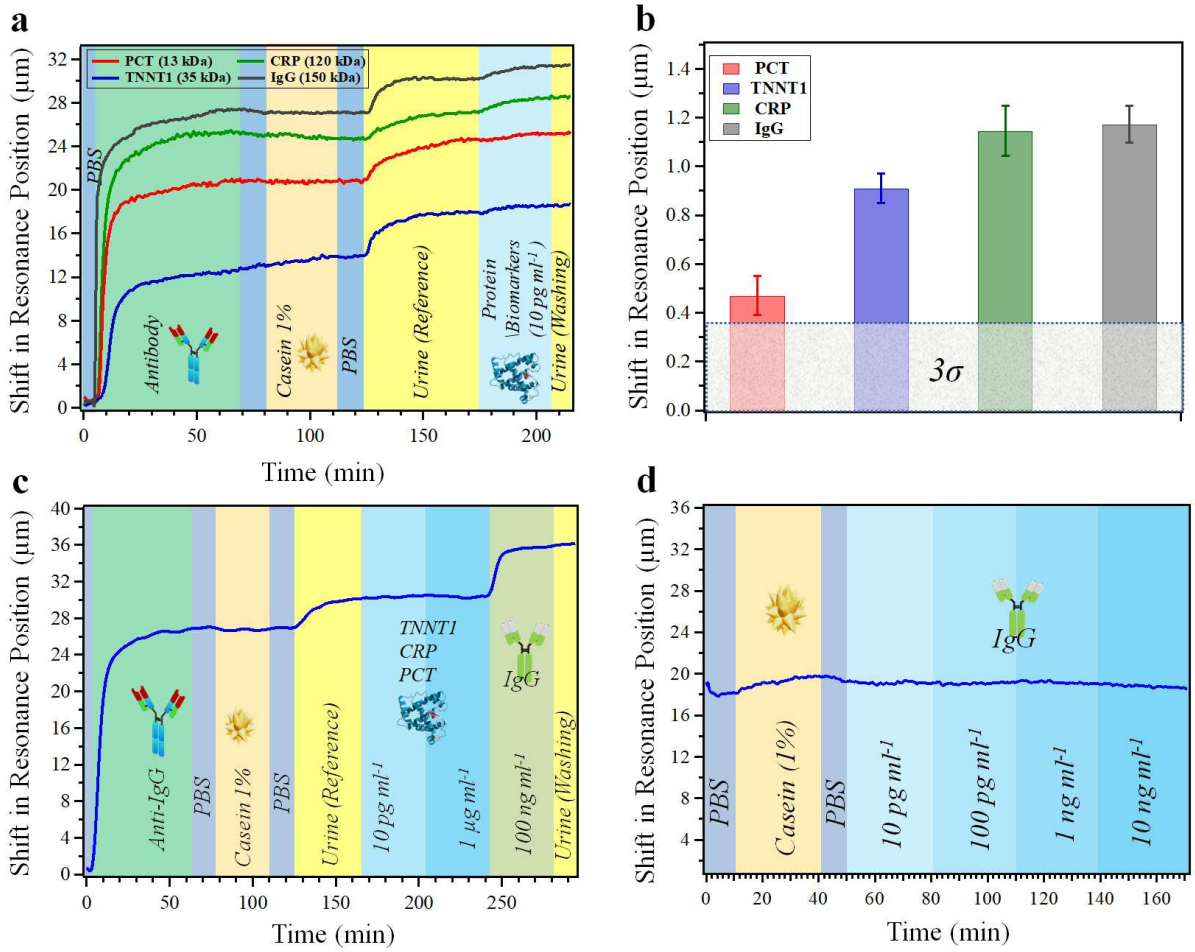

Fig. 4. Binding assay using PEGylated chirped GMR sensor. (a) Demonstration of binding assay conducted in urine (*pH* = 7.4), showing the shift in resonance position against time with each assay step. Each channel comprises a single antibody that is challenged with its associated, recombinant antigen. A clear binding curve is observed for each of the 4 proteins at a concentration of 10 pg mL^{-1}, i.e. procalcitonin (PCT), C-reactive protein (CRP), troponion (TNNT1), and Immunoglobulin G (IgG). (b) Comparison of the maximum shift observed for the 4 proteins, for a concentration of 10 pg mL^{-1}. Each point represents the mean ±SD of four replicates. The noise level value (3σ) is also indicated. (c) Controlled measurement, demonstrating that no binding is observed for mixture of TNNT1, CRP and PCT against an IgG antibody. (d) Similarly, no IgG binding is observed in the absence of a suitable antibody, demonstrating that the curves in (a) are not due to physisorption.

204 highlighting the density and anti-fouling properties of the PEG monolayer. Following antibody

functionalization, the four channels were exposed to urine which leads to a shift in resonance due to the higher refractive index; we see a similar effect in a control experiment conducted with PBS and urine in the absence of antibody (Fig. S5). Later, we add urine spiked with a recombinant protein biomarker at a concentration of 10 pg mL^{-1} and see clear shifts for all channels. The urine pH was adjusted by adding a few microliters of a strong base (NaOH) to 45 ml of urine, thus the dilution factor is negligible. It is worth noting that the binding efficiency of each antigen-antibody pair depends on the pH of the medium. While it would be ideal to optimize the pH for each channel, this would complicate sample preparation and would not be possible in a multiplexed format, so would be undesirable for point-of-care applications. Despite these limitations, our results show an excellent sensitivity at a single pH-value for all 4 antibody-antigen pairs.

IgG immunoassay is conducted in individual channel. We also used a reference channel to minimize the influence of temperature variations and background noise, by subtracting from the measurement channel, see supporting information (Fig. S6). Finally, a urine washing step is performed after the addition of biomarkers. No shift in the resonance position is observed, indicative of antibody-antigen binding rather than physisorption. Interestingly, these results are similar and within experimental error to those conducted in PBS rather than urine (Fig. S7), which again highlights the good surface coverage of the PEG and the suppression of non-specific binding. As urine typically contains a high level of salts, the ionic strength of the solution may impact on the weak non-covalent bond between antibody and antigen. We are therefore particularly pleased to note the high efficiency of the PEG-functionalised surface in terms of anchoring antibodies and enabling binding to their complementary antigens, even in a matrix of undiluted human urine. Fig. 4b shows the resonant shifts observed for 10 pg mL^{-1} of the four protein biomarkers (0.47 μm ±17 %, 0.91 μm ±7 % , 1.15 μm ±9 % , and 1.17 μm ±6 % for PCT, TNNT1, CRP, and IgG,

respectively). Since the GMR is a refractive index sensor, one would expect that the magnitude of the resonant shift would increase with molecular weight. This trend is observed qualitatively, i.e. the smallest molecule (PCT, 13 kDa) produces the smallest shift, and IgG (150 kDa) the largest, although as expected the difference does not scale quantitatively with mass. Finally, we add urine spiked with IgG, TNNT1, and PCT at concentrations ranging from 10 pg mL^{-1} up to 1 μg mL^{-1}, along with CRP at concentrations ranging from 1 pg mL^{-1} up to 1 μg mL^{-1} (Fig**.** S8).

Further controlled experiments confirm that we observe specific interactions between the immobilized antibodies and the associated antigen rather than physisorption. Firstly, we observe no shift in resonance when a sensor surface functionalized with anti-IGG is challenged with urine spiked with a mixture of TNNT1, CRP and PCT (Fig. 4c). When the same surface is subsequently exposed to IgG at 100 ng mL^{-1}, we observe a clear binding curve, highlighting that the antibody binding sites remain active following exposure to other proteins. Secondly, Fig. 4d shows a PEG functionalized but antibody-free surface exposed to IgG. No significant binding of IgG is observed. We therefore unambiguously demonstrate that the binding curves observed are due to the formation of an antibody-antigen complex.

3.3. Comparison to previous results

It is interesting to compare our result to competing approaches. Most notably, surface plasmon resonance (SPR) is considered by many as the gold standard for label-free sensing via photonic resonances. SPR-based biosensors have been reported that are capable of detecting protein biomarkers with a detection limit of 460 pg mL^{-1} in 1:1 diluted urine (Soler et al., 2016), and 140 pg mL^{-1} in PBS (Li et al., 2017). This comparison clearly shows that the GMR technology is highly competitive, especially in conjunction with the PEG surface functionalization protocol, which

offers highly efficient and selective binding of antigens while suppressing non-specific binding. More importantly, the performance we quote is comparable to the typical detection limit quoted for an enzyme-linked immunoassay (ELISA), the laboratory gold standard, which is in the low pg mL^{-1} range (Sui et al., 2006). This means that the intrinsically simple and label-free GMR approach achieves the same performance as a fluorescent label-based ELISA that requires trained laboratory personnel, which is quite remarkable.

4. Discussion

We have exploited the combined sensing and imaging capability of a chirped guided mode resonance sensor to demonstrate label-free detection of multiple disease-relevant proteins in undiluted human urine. Specifically, we have demonstrated the detection of four protein biomarkers, all at a limit of detection of better than 10 pg mL^{-1}. The high performance and ability to perform multiple tests in parallel is supported by the use of a $SM(PEG)_6$ spacer layer in the functionalization protocol which introduces steric freedom and permits the immobilization of antibodies at high density while minimizing nonspecific binding. We have verified this performance against comparable protocols using APTES and dextran that are typically used for dielectric sensor surfaces and have shown improved performance. A comparison against other photonic sensor modalities is made more difficult by the fact that most published results only refer to laboratory dilutions, which avoid nonspecific binding by the absence of competing agents, while our results are achieved in undiluted human urine. Moreover, our sensor and photonic readout mechanism is intrinsically low-cost and does not require careful alignment or expensive components, which sets it further apart. In this regard, it is particularly surprising that our label-free approach now achieves the same pg ml^{-1} performance as commercially available enzyme-linked immunoassays (ELISAs) that use labels and require trained laboratory personnel.

5. Conclusion

In conclusion, the parallel detection of 4 clinically relevant biomarkers in human urine, all at concentrations of 10 pg ml^{-1} or below, demonstrates that the guided mode resonance (GMR) sensing modality, together with a highly efficient PEGylation process for immobilizing antibodies, offers a favorable combination of properties for the realization of low-cost, high performance biosensors suitable for evaluating clinical samples. The technology is intrinsically simple, yet it is essential to demonstrate similar performance as shown here also in a handheld format and in a clinical setting in order to prove its true value as a point-of-care tool.

Conflicts of interest

The authors report no conflicts of interest in this work.

Acknowledgment

We acknowledge financial support by the Engineering and Physical Sciences Research Council of the UK through grants EP/P02324X/1 ("MAPS") and EP/P030017/1 ("Resonant Photonics"), as well as through the GrowMedTech initiative of the University of Leeds. TFK also acknowledges support through a Royal Society Wolfson fellowship and JS the National Key Research and Development Program of China (Grant No. 2017YFC1200904) and the National Natural Science Foundation of China (Grant Nos. 11761141006, 81822024, and 21605102).

Appendix A. Supplementary data

Supplementary data associated with this article can be found in the online version.

S1. Experimental section

S2. IgG binding assay for QCMD analysis using APTES, dextran, and $SM(PEG)_6$ protocols

References

Barnes, A.E., 1966. J. Immunol. 96, 854 LP – 864.

Cunningham, B.T., 2010. J. Assoc. Lab. Autom. 15, 120–135.

Dixit, C.K., Vashist, S.K., MacCraith, B.D., O'Kennedy, R., 2011. Nat. Protoc. 6, 439–445.

Drayton, A., Barth, I., Krauss, T.F., 2019. Semiconduct Semimet. 100, pp. 115–148.

Eamudomkarn, C., Sithithaworn, P., Kamamia, C., Yakovleva, A., Sithithaworn, J., Kaewkes, S., Techasen, A., Loilome, W., Yongvanit, P., Wangboon, C., Saichua, P., Itoh, M., M. Bethony, J., 2018. PLoS One 13, e0192598.

Herranz, S., Gavela, A.F., Lechuga, L.M., 2017. Biosensors and Biodetection: Methods and Protocols Volume 1: Optical-Based Detectors (Berlin: Springer) pp 161–85.

Hughes-Jones, N.C., Gardner, B., Telford, R., 1964. Immunology 7, 72–81.

Jönsson, C., Aronsson, M., Rundström, G., Pettersson, C., Mendel-Hartvig, I., Bakker, J., Martinsson, E., Liedberg, B., MacCraith, B., Öhman, O., Melin, J., 2008. Lab Chip 8, 1191.

Kazemi-Darsanaki, R., Azizzadeh, A., Nourbakhsh, M., Raeisi, G., AzizollahiAliabadi, M., 2013.

315 J. Biol. Today's World 2.
316 Kenaan, A., Nguyen, T.D., Dallaporta, H., Raimundo, J.-M., Charrier, A.M., 2016. Anal. Chem.
317 88, 3804–3809.
318 Kim, D., Herr, A.E., 2013. Biomicrofluidics 7, 041501.
319 Kuo, S.C., Lauffenburger, D.A., 1993. Biophys. J. 65, 2191–2200.
320 Lee, J.E., Seo, J.H., Kim, C.S., Kwon, Y., Ha, J.H., Choi, S.S., Cha, H.J., 2013. Korean J. Chem.
321 Eng. 30, 1934–1938.
322 Li, W., Prabakaran, P., Chen, W., Zhu, Z., Feng, Y., Dimitrov, D., 2016. Antibodies 5, 19.
323 Li, X., Soler, M., Özdemir, C.I., Belushkin, A., Yesilköy, F., Altug, H., 2017. Lab Chip 17, 2208–
324 2217.
325 Luchansky, M.S., Washburn, A.L., Martin, T.A., Iqbal, M., Gunn, L.C., Bailey, R.C., 2010.
326 Bioelectron. 26, 1283–1291.
327 Makaraviciute, A., Ramanaviciene, A., 2013. Biosens. Bioelectron. 50, 460–471.
328 Nagasaki, Y., Kobayashi, H., Katsuyama, Y., Jomura, T., Sakura, T., 2007. J. Colloid Interface Sci.
329 309, 524–530.
330 Pochechueva, T., Chinarev, A., Bovin, N., Fedier, A., Jacob, F., Heinzelmann-Schwarz, V., 2014.
331 J. Immunol. Methods 412, 42–52.
332 Soler, M., Estevez, M.-C., Moreno, M. de L., Cebolla, A., Lechuga, L.M., 2016. Biosens.
333 Bioelectron. 79, 158–164.
334 Stefansson, S., Kwon, H.H., Ahn, S.N., 2012. J. Nanotechnol. 2012, 1–8.
335 Strauch, E.-M., Fleishman, S.J., Baker, D., 2014. Proc. Natl. Acad. Sci. 111, 675–680.
336 Sui, G., Wang, J., Lee, C.-C., Lu, W., Lee, S.P., Leyton, J. V., Wu, A.M., Tseng, H.-R., 2006. Anal.
337 Chem. 78, 5543–5551.
338 Tanislav, C., Guenduez, D., Liebetrau, C., Giese, A.K., Eichler, S., Sieweke, N., Speth, M., Bauer,

T., Hamm, C., Rolfs, A., 2016. PLoS One 11, e0157640.

Thakur, M.S., Ragavan, K. V., 2013. J. Food Sci. Technol. 50, 625–641.

Thévenot, D.R., Toth, K., Durst, R.A., Wilson, G.S., 2001. Biosens. Bioelectron. 16, 121–31.

Triggs, G.J., Wang, Y., Reardon, C.P., Fischer, M., Evans, G.J.O., Krauss, T.F., 2017. Optica 4, 229.

Upasham, S., Tanak, A., Prasad, S., 2018. Adv. Heal. Care Technol. Volume 4, 1–13.

Vashist, S.K., 2012. Diagnostics 2, 23–33.

Wang, S.S., Magnusson, R., 1993. Appl. Opt. 32, 2606.

Wawro, D.D., Tibuleac, S., Magnusson, R., Liu, H., 2000. Proc. SPIE, 3911, 86-94

Weimer, B.C., Walsh, M.K., Wang, X., 2000. J. Biochem. Biophys. Methods 45, 211–9.

Wen, X., He, H., Lee, L.J., 2009. J. Immunol. Methods 350, 97–105.

Yakovleva, J., Davidsson, R., Bengtsson, M., Laurell, T., Emnéus, J., 2003. Bioelectron. 19, 21–34.

Yang, D., Giragossian, C., Castellano, S., Lasaro, M., Xiao, H., Saraf, H., Hess Kenny, C., Rybina, I., Huang, Z.-F., Ahlberg, J., Bigwarfe, T., Myzithras, M., Waltz, E., Roberts, S., Kroe-Barrett, R., Singh, S., 2017. MAbs 9, 1105–1117.

Yuan, Y., Zhang, J., Yin, M., Liu, C., 2014. Adv. Biomater. 2014, 1–8.

358

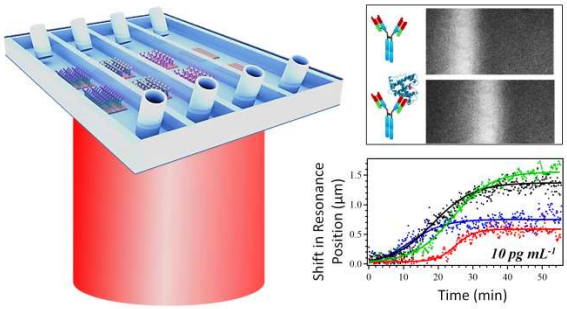

359 TOC figure